Magnesium-Induced Lipid Bilayer Microdomain Reorganizations: Implications for Membrane Fusion

ARTICLE *in* THE JOURNAL OF PHYSICAL CHEMISTRY B · AUGUST 2009

Impact Factor: 3.3 · DOI: 10.1021/jp9011944 · Source: PubMed

5 AUTHORS, INCLUDING:

Zachary D Schultz
University of Notre Dame
47 PUBLICATIONS **480** CITATIONS
SEE PROFILE

Ileana Pazos
University of Pennsylvania
11 PUBLICATIONS **123** CITATIONS
SEE PROFILE

E. Neil Lewis
Malvern Instruments
126 PUBLICATIONS **2,359** CITATIONS
SEE PROFILE

Published in final edited form as:
J Phys Chem B. 2009 July 23; 113(29): 9932–9941. doi:10.1021/jp9011944.

Magnesium Induced Lipid Bilayer Microdomain Reorganizations: Implications for Membrane Fusion

Zachary D. Schultz[1], **Ileana M. Pazos**[1], **Fraser K. McNeil-Watson**[2], **E. Neil Lewis**[2], and **Ira W. Levin**[1,*]

[1]Laboratory of Chemical Physics, National Institutes of Diabetes and Digestive and Kidney Diseases, National Institutes of Health, Bethesda, MD, 20892

[2]Novel Measurements Group, Malvern Instruments, Ltd., Malvern WR14 1XZ, United Kingdom

Abstract

Interactions between dipalmitoylphosphatidylcholine (DPPC) and dipalmitoylphosphatidylserine (DPPS), combined both as binary lipid bilayer assemblies and separately, under the influence of divalent Mg^{2+}, a membrane bilayer fusogenic agent, are reported. Infrared vibrational spectroscopic analyses of the lipid acyl chain methylene symmetric stretching modes indicate that aggregates of the two phospholipid components exist as domains heterogeneously distributed throughout the binary bilayer system. In the presence of Mg^{2+}, DPPS maintains an ordered orthorhombic subcell gel phase structure through the phase transition temperature, while the DPPC component is only minimally perturbed with respect to the gel to liquid crystalline phase change. The addition of Mg^{2+} induces a reorganization of the lipid domains in which the gel phase acyl chain planes rearrange from an hexagonal configuration toward a triclinic, parallel chain subcell. Examination of the acyl chain methylene deformation modes at low temperatures allows a determination of DPPS microdomain sizes, which decrease in size upon the addition of DPPC-d_{62} in the absence of Mg^{2+}. On adding Mg^{2+}, a uniform DPPS domain size is observed in the binary mixtures. In either the presence or absence of Mg^{2+}, DPPC-d_{62} aggregates remain in a configuration for which microdomain sizes are not spectroscopically measurable. Analysis of the acyl chain methylene deformation modes for DPPC-d_{62} in the binary system suggests that clusters of the deuterated lipids are distributed throughout the DPPS matrix. Light scattering and fluorescence measurements indicate that Mg^{2+} induces both the aggregation and the fusion of the lipid assemblies as a function of the ratio of DPPS to DPPC. The structural reorganizations of the lipid microdomains within the DPPS/DPPC bilayer are interpreted in the context of current concepts regarding lipid bilayer fusion.

Keywords

Lipid microdomains; vesicle fusion; vibrational spectroscopy; light scattering; fluorescence; Mg

1. Introduction

The role of lipids in regulating cellular membranes has evolved greatly from the model of a homogeneous, fluid barrier supporting proteins to current concepts in which lipid and protein microdomains control cellular activities. Although controversial, a current concept invokes microdomain complexes, commonly referred to as “rafts”, to explain a variety of membrane

*Corresponding author: iwl@helix.nih.gov.
Laboratory of Chemical Physics, National Institutes of Diabetes and Digestive and Kidney Diseases, National Institutes of Health, Bethesda, MD, 20892

associated phenomena.[1–5] Efforts to detect and to characterize these lipid raft domains in intact membranes led to the consideration that numerous bilayer microdomains, in addition to raft-type structures, exist in biological membranes, thus emphasizing the "mosaicism" of the Singer-Nicholson model to better reflect the current understanding of membrane bilayer architecture.[5] The existence of raft-like domains is derived from the observation of detergent insoluble membrane fractions[6] even though it remains difficult to observe directly these microdomains in intact cellular systems. Model systems, however, demonstrate the chemical interactions giving rise to membrane microdomains, and provide progress toward understanding the effects of domain organizational changes as they relate to complex biological phenomena.[7–13]

Since domains may form in response to a stimulus,[1] issues arise in relation to specific stimulus driven bilayer reorganizations, such as biomembrane fusion. Membrane bilayer fusion represents important processes in many biochemical and biophysical events, including cellular signaling and trafficking. Both theoretical[14–16] and experimental models for elucidating lipid bilayer fusion have been proposed. A classic lipid vesicle fusion assay monitors the exchange of encapsulated fluorescent dyes between phosphatidylserine (PS) vesicles in the presence of Ca^{2+} and Mg^{2+} cations.[17] Bilayer fusion has also been observed from vesicles formed from oppositely charged fluorescent lipids.[18] A common characteristic of these vesicle fusion assays is that increased concentrations of zwitterionic lipids, such as phosphatidylcholine (PC), inhibit PS fusion, or only allows a fusion of the outer leaflet without bridging the vesicle's internal contents.[17,18] Changes in lipid composition, such as differing length acyl chain lengths[19] or the inclusion of unsaturated chain lipid species,[20] are reported to modulate fusion properties; however other perturbations, as, for example, changes in pH,[21,22] the insertion of either small peptides[23] or polyethyleneglycol molecules,[24,25] also affect the fusion process.

Experimental studies generally assess either the success or failure of fusion; however, experimental evidence concerning specific lipid interactions within the bilayer during the fusion process is limited. Towards this end, numerous approaches, in addition to the fluorescence experiments noted above, have been attempted, including, for example, electrical conductance measurements,[26] calorimetry,[23,27] and light scattering methods.[28,29] Lateral phase separation has been studied for various lipids associated with the fusion process.[19,30,31] X-ray diffraction experiments have successfully detected partial fusion, or hemifusion, events in lipid bilayer assemblies [32,33]. Vibrational infrared spectroscopic techniques, however, suggest an additional and potentially important mechanistic approach toward characterizing bilayer fusion properties, particularly, since lipid acyl chain packing configurations[34] and temperature dependent rearrangements can be readily gauged.[27] Specifically, infrared spectroscopy has been used successfully to monitor phase changes associated with lipid bilayer inhomogenieties and headgroup/ interfacial – ion interactions.[27,35,36] For bovine brain DPPS assemblies, an infrared spectroscopic analysis of changes in the phosphate bands indicated that divalent cations bind to the phosphate in a bidentate configuration; upon binding Ca^{2+}, a fusogenic agent, the gel to liquid crystalline phase transition of bovine brain DPPS was observed to be suppressed to temperatures greater than 100 °C.[37]

In the present study we apply infrared spectroscopic techniques to examine the binary DPPS/DPPC bilayer system both for assessing bilayer microdomain formation and for determining lipid acyl chain reorganizations within the membrane's hydrophobic core in response to a divalent cation fusion catalyst, namely, Mg^{2+}. In our model systems, we utilize disaturated palmitoyl acyl chain lipids in order to facilitate microdomain characterizations. In particular, the observed bilayer reorganizations reveal putative interactions involved in disrupting the bilayer membrane as the fusion process progresses. We augment the infrared spectroscopic

measurements with dynamic light scattering studies and fluorescence determinations for further characterization of the bilayer fusion event.

2. Experimental Methods

Materials

1,2-dipalmitoyl-sn-glycero-3-phosphocholine (DPPC), 1,2-dipalmitoyl-d_{62}-sn-glycero-3-phosphocholine (DPPC-d_{62}), and 1,2-dipalmitoyl-sn-glycero-3-[phospho-l-serine] (sodium salt) (DPPS) were purchased from Avanti Polar Lipids (Alabaster, AL). All multilamellar and unilamellar lipid bilayer assemblies were prepared using ultra pure water (KD Medical, Columbia, MD). Stock solutions of molecular biology grade 1.0 M $MgCl_2$ and 0.5 M ethylenediaminetetraacetic acid (EDTA, pH = 8.0) in H_2O were obtained from Quality Biological, Inc. (Gaithersburg, MD) and diluted as necessary. HPLC grade chloroform was procured from Sigma-Aldrich (St. Louis, MO).

Sample Preparation

Multilamellar lipid vesicles (MLVs) were prepared from appropriate mole fractions of DPPS and DPPC lipids. For infrared spectroscopic experiments, DPPC-d_{62} was used to permit chain discrimination from the DPPS components. Mixed lipid systems were prepared from stock solutions in chloroform. Chloroform was removed by flowing nitrogen gas over the samples followed by maintaining the mixtures under vacuum overnight. Lipid mixtures were dispersed in either ultrapure H_2O or phosphate buffered saline, pH 7–7.4, to produce MLVs with approximately 25% (wt.%) lipid. For infrared experiments, MLV dispersions were sandwiched between two ZnSe windows and transferred to the infrared spectrometer. For light scattering and vesicle fusion assays, the MLVs were diluted to 1% (wt. %) and sequentially extruded through 1.0 μm, 0.4 μm, 0.2 μm, and 0.1 μm Whatman Nuclepore Track-Etch polycarbonate membranes (Whatman plc., Kent, UK) to obtain unilamellar vesicles (SUVs) of approximately 100 nm in diameter.

Infrared Spectroscopy

Temperature dependent infrared vibrational spectra were collected using a liquid nitrogen gas exchange cryostat mounted on a DA-3 Bomem infrared spectrometer. Infrared spectra were acquired with 0.5 cm^{-1} spectral resolution and using Hamming apodization. Infrared spectra of the lipid MLVs were acquired at 25 °C. Domain size and organization were charactized in detail using a rapid quenching spectroscopic methodology described previously.[38] Briefly, lipids were rapidly cooled from the liquid crystalline to the gel phase, reaching a final −120 °C within minutes. Correlation field splitting parameters involving the methylene deformation modes were obtained at −120 °C; the samples were then heated at various temperature intervals for collecting spectra to ascertain temperature dependent spectral changes and to obtain phase transition information.

Infrared spectroscopic correlation field splitting parameters were determined from curve deconvolutions corresponding to minima observed in the second derivative spectra in the 1470 cm^{-1} and 1090 cm^{-1} spectral regions representative of the methylene deformation modes for the normal protonated and perdeuterated acyl chain systems, respectively. Melting curves were generated from the temperature dependent frequencies of the 2850 cm^{-1} and 2090 cm^{-1} methylene symmetric stretching modes of the respective lipid species. Peak frequencies were determined to better than ± 0.1 cm^{-1} from the fits of Lorentzian bandshapes with appropriate baseline corrections. Peak fitting was accomplished using Grams 7.0 (Thermo-Galatic Inc.). Gel to liquid crystalline phase transition temperatures (T_ms) and phase transition intervals (ΔT) for each melting curve were determined using a previously described two-state model.[39]

Dynamic Light Scattering

To measure the extent of irreversible vesicle aggregation, a light scattering size assay was employed. Particle size measurements were obtained using a Malvern Instruments LTD, Zetasizer Nano (Malvern, UK). SUVs prepared by extrusion were diluted to a concentration of 0.45 mg/mL (total lipid weight to volume). 1 mL of lipid solution was added to a standard 1 cm cuvette. The initial vesicle size distribution was obtained. Samples were prepared with an initial polydispersity index (PDI) of 0.1 or better. Mg^{2+} titration was performed by addition of either a single 100 μL aliquot or a series of 10 × 10 μL aliquots of 10 mM MgCl solution to the cuvette containing SUVs. After each addition the sample was gently stirred and a particle size measurement obtained. After the addition of 100 μL of Mg^{2+}, the solution was back titrated with the addition of 20 μL of 100 mM EDTA solution (pH=8.0), and the particle size distribution was measured. All measurements were determined at 25 °C.

The data were analyzed using the Dispersion Technology Software v.5.1 beta (Malvern Instruments, LTD.) Dynamic light scattering data were collected at a scattering angle of 173 degrees from a laser source of 633 nm wavelength. The particle size distribution was derived from the diffusion coefficient distribution, which is characterized by fitting a set of exponential decays to the first order homodyne correlation function, with non-negativity and smoothness constraints. The algorithm used is capable of quantifying multimodal decay spectra, such as those occurring in particle size distributions, subject to the constraint that the sizes are separated from an adjacent component by a factor of approximately 2.[40] It is also necessary to verify that sample concentrations avoid complications that arise from multiple scattering and particle interactions. Such ideal behavior is determined by experimental measurements over a range of concentrations for the dispersed phase and by selecting the range over which the result is independent of sample concentration. In this work the peak representing the most substantial size component (or the only component) was used to characterize the ‘particle size’ of the sample.

Fluorescence Imaging

Multilamellar vesicles were prepared in 0.1 M saline solutions containing 0.1 mM of either 6-carboxyfluorescein (6-CF) or sulforhodamine 101 (SR101) fluorescent indicators (Sigma Aldrich, St. Louis, MO). 5 μm vesicles were prepared by extrusion of the multilamellar vesicles in the fluorescent molecule solution through a polycarbonate membrane with 5 μm pore size. The fluorescent indicator containing vesicles were then isolated from excess fluorescent indicator by passing the vesicle solution through a Sephadex G-25 Superfine column (GE Healthcare, Piscataway, NJ). The 6-CF and SR101 containing vesicles were combined in the presence of 1 mM Mg^{2+}. After 15 min, the mixed vesicle solution was suspended in 2% agarose and imaged under a microscope. The fluorescence assay was performed at room temperature, nominally 21–25 °C.

3. Results

A. Phase Transition Characteristics

Melting curves were constructed from the changes in the frequencies of the acyl chain methylene symmetric stretching modes for multilamellar assemblies of both pure DPPS and DPPC, as well as mixed lipid systems comprised of 9:1, 3:1, and 1:1 mole fractions of DPPS to DPPC-d_{62}, respectively. The perdeuterated DPPC acyl chains permit discrimination between the DPPC and DPPS components. The DPPS acyl chain methylene symmetric stretching modes at 2850 cm^{-1} shift to 2090 cm^{-1} in the deuterated DPPC system. The gel to liquid crystalline phase transition curves, shown in figure 1, plot the changes in the symmetric stretching mode frequencies as a function of temperature for DPPS (Fig 1A) and DPPC-d_{62} (Fig 1B) in the pure and binary systems.

Several trends are evident in Figure 1A. First, the methylene symmetric stretching mode frequencies are slightly lower both in the gel and liquid crystalline phase for the 9:1 DPPS-DPPC mixture in comparison to pure DPPS, indicating a more ordered acyl chain system. In contrast, increasing amounts of DPPC-d_{62} in the binary mixtures increases the frequency of the methylene symmetric stretching modes in both the gel and liquid crystalline phases. This increased frequency in the binary systems is commonly associated with increasing chain disorder in comparison to pure DPPS, but has also been attributed to changes in vibrational coupling associated with isotopic dilution.[41] A second trend evident in Figure 1A is the shift in the gel to liquid crystalline T_m of the DPPS component with increasing DPPC-d_{62} content. Table 1 records the phase transition temperature, T_m, and transition width, ΔT values determined for all samples explored in this study. The gel to liquid crystalline transition is observed to be sharp, occurring over less than 1° C, for pure DPPS, but broadens with increased DPPC-d_{62} content. In the 1:1 mixtures, the melting transition is observed over a temperature interval of nearly 10°.

The phase transition profiles for the DPPC-d_{62} component of the binary system are plotted in Figure 1B. Contrary to the trend observed for DPPS, the gel phase disorder, which is slightly greater than pure DPPC-d_{62}, remains nearly constant for the DPPS-DPPC-d_{62} mixtures. DPPC-d_{62} shows an increase in T_m, compared to the pure MLV, with increasing DPPS content and is consistent with the T_ms of the DPPS component. The T_ms, summarized in Table 1, indicate that the phase transition temperatures of DPPC-d_{62} in the binary systems are significantly higher than pure DPPC-d_{62}. In the binary systems, the DPPC-d_{62} T_m is observed to occur at temperatures slightly below the DPPS melting transition. In the 1:1 system, the melting temperature of DPPC-d_{62} is observed about 2.5° below that of the DPPS component. A similar result was reported for the T_ms of a 1:1 mixture of perdeuterated dimyristoylphosphatidylcholine (DMPC-d_{54}) and dimyristoylphosphatidylserine (DMPS).[27] While the exact T_ms are slightly different for the DPPS and DPPC-d_{62} components, the shapes of the melting curves exhibit strong similarities. The narrow widths of the melting transitions, ΔT, indicate that the pure lipid systems show a high degree of cooperativity. The broad transitions observed in the mixed lipid systems indicate a loss of cooperativity. A similar melting transition for a 1:1 mixture of DPPS and DPPC was observed over the same broad temperature window (ca. 10°) using calorimetry,[23] as was observed in our study. The broadened temperature profiles for the binary systems also agree with the phase diagram reported from electron paramagnetic resonance experiments.[31] The T_m's for the pure lipid components are consistent with values previously reported.[42] The broadening of the phase transition widths observed in melting curves for the binary systems is consistent with the formation of lipid microdomain components that undergo their phase transitions at slightly different temperatures. The general T_ms for the binary system are driven by the phase transition for the DPPS component. Interestingly, Monte-Carlo[43,44] and molecular dynamics[45] simulations suggest PS and PC mixtures exhibit non-ideal mixing which leads to lipid clustering. The ΔTs observed in the infrared spectroscopic melting curves supports the idea of randomly distributed lipid clusters comprising the bilayer assemblies.

The addition of Mg^{2+}, shown in Figure 2, has dramatic effects on the phase transition behavior, particularly that of DPPS (Fig 2A). Lipid samples were prepared in $MgCl_2$ solution, to yield a lipid to Mg^{2+} mole ratio of 1:1.5, providing a slight molar excess of Mg^{2+}. In the presence of Mg^{2+}, DPPS acyl chains maintain an ordered gel phase across the conventional phase transition temperature that occurs without Mg^{2+}. Conversely, the DPPC-d_{62} acyl chains continue to exhibit a gel to liquid crystalline phase change, as shown in Figure 2B, indicating independent DPPC-d_{62} microdomains. In Table 1, the T_ms of the DPPC-d_{62} component is observed at temperatures 1–1.5° lower in the binary lipid systems containing Mg^{2+}, but 2.5° higher in the pure DPPC-d_{62} + Mg^{2+} system. This 2.5° elevated melting temperature for pure DPPC-d_{62} is consistent with the behavior of lipids in the presence of salts.[42] The width of the

DPPC-d_{62} melting transitions is observed to be broader in the presence of Mg^{2+}, despite the close correspondence in T_ms to the melting curves without Mg^{2+}. These increased ΔT values indicate that the DPPC-d_{62} component lipids behave less cooperatively and more independently than the DPPS component in the presence of Mg^{2+}; however, the elevated T_ms for DPPC-d^{62} components in the binary systems suggest that the DPPS matrix exerts a force on the DPPC microdomains inhibiting disorder until higher temperatures are obtained. This further implies that DPPC lipid clusters remain randomly distributed throughout the DPPS matrix. Had Mg^{2+} induced a complete phase separation, one would expect see the DPPC-d_{62} acyl chains behave in a fashion similar to pure DPPC-d_{62}. Experiments performed using additional monovalent Na^+ and K^+ salts, showed no significant differences in the phase transition curves from that of pure H_2O.

Inspection of the phosphate asymmetric stretching mode provides insight into the nature of Mg^{2+} binding to the DPPS present in the bilayer assemblies. In aqueous assemblies, this phosphate stretching mode is observed as a broad band at 1224 cm^{-1} (see Supporting Information). Addition of Mg^{2+} results in a shift in this mode to 1242 cm^{-1} (see Supporting Information). This frequency shift is known to correspond to binding between the phosphate moiety and a divalent cation, which also results in dehydration of the phosphate in the lipid headgroup.[37] No shift is observed for pure DPPC-d_{62} assemblies (see Supporting Information), further indicating the Mg^{2+} interacts specifically with DPPS.

B. Lipid Bilayer Microdomain Characterization in MLVs

Examination of the methylene deformation modes provides insight into the acyl chain packing properties and the existence of lipid microdomains. In Figure 3, the methylene deformation modes at ~1467 cm^{-1} for DPPS and ~1090 cm^{-1} for DPPC-d_{62} are plotted at 25 °C for the different lipid assemblies with and without Mg^{2+}. Figure 3A for pure DPPS at 25 °C, shows a chain packing configuration to be a convolution of hexagonal chain organization, represented by a peak at 1467 cm^{-1}, and an orthorhombic subcell, which results in a split peak accounting for the shoulders at higher and lower frequencies. The addition of DPPC-d_{62} disrupts the gel phase orthorhombic chain packing order in which the frequency of the methylene deformation modes shift to higher frequencies with increasing amounts of DPPC-d_{62}, from 1467 cm^{-1} for the hexagonal subcell of pure DPPS to 1469 cm^{-1} for the 1:1 mixture with DPPC-d_{62}. Examination of the deuterated methylene deformation modes of DPPC-d_{62} in Figure 3B shows only a broad single peak at 1089 cm^{-1}, representative of a hexagonally organized gel phase chain subcell. In Figure 3B the spectra are normalized to the 1089 cm^{-1} peak intensity. For the 9:1 DPPS-DPPC-d_{62} mixture, the low signal attendant to the small DPPC-d_{62} component is barely visible above the background; however, the peak position is clearly determined from a second derivative spectral analysis.

The addition of Mg^{2+} dramatically alters the acyl chain packing characteristics as seen in Figures 3C and 3D. Two spectral features are worth particular note in Figure 3C. First, definitive splitting, representative of orthorhombic subcell lipid packing arrangements, is clearly observed in the pure DPPS system, replacing the hexagonal packing system originally observed in the absence of Mg^{2+}. A small hexagonal spectral component is still evident, although largely diminished. Shoulders are observed in the binary assemblies, representative of splitting patterns. Second, the DPPS-DPPC-d_{62} mixtures all exhibit nearly identical spectra. DPPC-d_{62} in Figure 3D demonstrates a different behavior than that observed for DPPS in that the pure DPPC-d_{62} assembly is unaffected by the addition of Mg^{2+}. The mixed DPPS-DPPC-d_{62} systems exhibit a single peak shifted to 1092 cm^{-1}. Previous studies indicate that in protonated lipid systems the occurrence of a single peak at 1473 cm^{-1} for the methylene deformation mode, compared to 1467 cm^{-1} for an hexagonal chain packing arrangement, is indicative of a triclinic subcell in which the acyl chain planes are arranged in a parallel manner.

[46] Accounting for the expected shift in frequency attendant to isotopic substitution, the peak at 1092 cm^{-1} of DPPC-d_{62} corresponds well with the triclinic subcell organization.

Correlation field splitting parameters for the methylene modes are enhanced at low temperatures. That is, in order to capture the liquid crystalline clustering characteristics, we employed the rapid quenching methodology from the high temperature phase, which was previously established for investigation of lipid microdomains,[38] to obtain correlation field splitting parameters from spectra at −120 °C. Figure 4 displays the low temperature spectra of the methylene deformation mode both in the absence (Figs 4A and 4B) and presence (Fig 4C and 4D) of Mg^{2+} for the DPPS and DPPC-d_{62} chains, respectively. As expected, DPPS in Figure 4A exhibits an orthorhombic chain packing arrangement, as evidenced by the observation of correlation field splitting components, in all samples. Microdomain sizes can be estimated from the relationship:

$$N=\left[\frac{\pi}{\sqrt{2(1-\Delta\nu/\Delta\nu_0)}}-1\right]^2, \quad \text{(Eq. 1)}$$

where Δν is the observed correlation field splitting and $\Delta\ \nu_0$ is the reference splitting observed from a pure assembly.[47] The number of interacting acyl chains (N) indicates that the microdomain sizes decrease as the percentage of DPPS decreases. In the 9:1 DPPS-DPPC-d_{62} assembly, the observed splitting is too large to accurately assess a domain size.[47] At lower DPPS concentrations, microdomains of 30 and 8 acyl chains are observed for the 3:1 and 1:1 DPPS-DPPC-d_{62} systems, respectively. The setting angle, the angle of the acyl chain carbon-carbon backbone plane with respect to the orthorhombic subcell axis, can be determined from the intensity ratio of the correlation field splitting components as follows[48]:

$$\cot(\theta)=\sqrt{\frac{I_a}{I_b}}, \quad \text{(Eq. 2)}$$

In equation 2, the I_a and I_b are the intensities of the high and low frequency splitting components, respectively. The intensities of the correlation field splitting components indicate setting angles representative of a slightly distorted orthorhombic subcell with respect to the ideal orthorhombic subcell setting angle of 45°. The low temperature correlation field splitting parameters, determined from peak deconvolutions, are listed in Table 2. The broad bandshapes observed in Figure 4B for DPPC-d_{62} in the 9:1 and 3:1 mixed lipid assemblies are not amenable to deconvolution to determine splitting components. However, a splitting is observed for the 1:1 mixed assembly and for the pure DPPC-d_{62} methylene deformation modes. The lack of splitting in the 9:1 and 3:1 mixed systems indicates that the DPPC-d_{62} lipid molecules are spatially isolated from each other or arranged in a random configuration that does not give rise correlation field interactions. In the 1:1 DPPS-DPPC-d_{62} mixture, there is some evidence of a small peak splitting, indicating that at higher DPPC concentrations splitting parameters would be observed.

Analysis of the low temperature correlation field splitting parameters in the presence of Mg^{2+} shows significant changes in the correlation field splitting components of DPPS (Fig. 4C). Both the magnitude of the splitting and the intensity of the splitting components are altered. From the N values tabulated in Table 2, Mg^{2+} addition results in the clustering of DPPS lipids. In the pure lipid system with added Mg^{2+}, microdomains of approximately 30 acyl chains are observed, while the mixed lipid systems with Mg^{2+} show a uniform domain size of approximately 20 acyl chains. The low frequency correlation field splitting component shows decreased intensity, resulting in a decreased setting angle for the DPPS systems. Interestingly,

the high frequency correlation field splitting component is observed at 1473 cm^{-1}. The observation of a single, unsplit, methylene deformation mode at this frequency indicates a triclinic chain plane subcell packing configuration. The dramatic change in setting angle in conjunction with observation of this 1473 cm^{-1} frequency suggests that Mg^{2+} induces the clustered DPPS chain planes to orient more parallel to each other.

Figure 4D shows the effect of Mg^{2+} addition on DPPC-d_{62}. The pure DPPC systems shows little change relative to the Mg^{2+} free system. This is consistent with the melting curve data above. The mixed lipid assemblies show an interesting change similar to their behavior at 25 °C, in which the deuterated methylene deformation modes are observed as a single peak shifted to a higher frequency. Accounting for the change in reduced mass attendant to the DPPC-d_{62} moiety, this shift is that which is expected for the triclinic, parallel chain plane, subcell arrangement. While the conformation of the dilute DPPC-d_{62} assemblies did not show strong organization in the absence of Mg^{2+}, in the presence of Mg^{2+} the DPPC-d_{62} component clearly demonstrates a triclinic organization in all the binary assemblies. Since the DPPC-d_{62} lipid shows no specific interaction with Mg^{2+}, the change in DPPC-d_{62} acyl chain organization in the mixed assemblies must arise from forces imposed on the bilayer by the DPPS Mg^{2+} interaction. Thus, the acyl chains of DPPC in the mixed systems remain randomly incorporated in the DPPS matrix and cluster in an orientation dictated by the DPPS acyl chains interacting with Mg^{2+}. Since the clusters exhibit a triclinic chain plane structure, infrared spectroscopy cannot determine a DPPC-d_{62} microdomain size.

C. Aggregation and Fusion Properties of Single Shell Vesicles

At 25 °C, DPPC and DPPS exist in a hydrated gel phase. To assess the reversibility of aggregation and possible fusion for these lipid assemblies, 100 μL of 10 mM Mg^{2+} was added in a single addition, followed by back titration with excess EDTA. Figure 5 displays the effect of Mg^{2+} and EDTA on the observed vesicle size distribution for each lipid system. In particular, all 5 samples show similar initial distributions of 100 nm single shell vesicles. The addition of Mg^{2+} results in an aggregation trend similar to that observed in the step-wise titration. The width of the distributions suggests that multi-aggregates may be forming, which appear to be more prevalent with increased DPPS concentration. EDTA is strong metal chelating agent, with a Mg^{2+} binding constant more than 2 orders of magnitude stronger than DPPS. Addition of excess EDTA is expected to remove Mg^{2+} from solution and to permit an assessment of aggregation reversibility. The addition of excess EDTA (relative to added Mg^{2+}) results in a slight size decrease for DPPS as well as the 9:1 and 3:1 DPPS-DPPC mixed vesicles. Upon standing for several hours, no further decrease in size was observed. The inability to recover the initial vesicle size distributions after treatment with EDTA implies vesicle fusion. The 1:1, DPPS: DPPC, system showed reversible aggregation, returning back to the original size distribution suggesting that in the 1:1 DPPS to DPPC mixed vesicle ensemble, Mg^{2+} induces vesicle aggregation without a fusion event. As expected, the Mg^{2+} or EDTA additions show little effect on the DPPC control sample. It has been previously demonstrated using a fluorescence-based mixing assay that increasing the amount of phosphatidylcholine within phosphatidylserine vesicles inhibits vesicle fusion;[17] the results presented here are consistent with the previous fluorescence data.

A fluorescent mixing experiment verified that both aggregation and fusion indeed occur. Figure 6 shows vesicle products that were imaged after mixing DPPS vesicles containing 6-CF and SR101 fluorescent indicators in the presence of 1 mM Mg^{2+}. In Figure 6a, it was observed that some vesicles showed colocalization of the fluorescent dyes indicating fusion. Aggregation was also observed, consistent with the light scattering results. Colocalization of these dyes was verified by examining the individual channels for SR101 (Figure 6b) and 6-CF (figure 6c). Single shell DPPS and binary DPPS/DPPC vesicles were observed to coalesce upon the

addition of Mg^{2+} by light scattering. The addition of EDTA, with a substantially stronger affinity for Mg^{2+} than either lipid, effectively removes the Mg^{2+} from solution. The fluorescence data indicates the irreversible increase in vesicle size under these conditions corresponds to vesicle fusion. The behavior observed from the gel phase di-saturated lipids is consistent with the behavior reported for the fluid phase bovine brain PS model systems reported previously.[17,37]

4. Discussion

The existence and behavior of membrane bilayer lipid microdomains and acyl chain plane reorganizations provide additional prospectives in our understanding of biomembrane fusion processes. Earlier studies investigating divalent cation induced PS and PC phase separation as a mechanism for fusion suggested that the concentration of PS lipids in *in-vivo* membranes was too low to drive the fusion process.[19] With the formation of lipid microdomains, however, the local, increased concentrations of specfic lipid components could allow fusion to occur. Previous reports indicate that the lipid bilayer must undergo significant changes in the kinetic steps toward complete fusion, some of which appear to incur substantial energetic penalties. Bilayer alterations toward complete fusion involve the initial contact between bilayers (or stalk formation), which entails the lipids to undergo significant conformational changes which could include bilayer stretching, chain tilting and bilayer bending deformations for accomplishing fusion without creating energetically unfavorable voids.[49] Since PS containing lipid vesicles are known to fuse in presence of Mg^{2+},[17] microdomain formation and subtle chain plane rearrangements provide a rationale for a detailed molecular basis for lipid bilayers undergoing fusion in a protein free model system.

There exists a long history of investigations into the binding of divalent cations to PS containing lipid.assemblies related to bilayer fusion.[17,19,50–57] Ca^{2+}, is reported to be a critical component in the membrane fusion process. Studies have shown that SNARE mediated bilayer fusion is dependent upon the presence of Ca^{2+} to complete the fusion process.[54,58,59] In another biological system, a Ca^{2+} release has been shown to trigger the release of sea urchin oocytes through via an excytotic membrane fusion event.[60] Both Ca^{2+} and Mg^{2+} are known to promote the fusion of lipid vesicles. It is now clear that molecular interactions involving the divalent cation are involved in the destabilization of the lipid bilayer necessary for fusion and that the binding of divalent cations to the lipid bilayer causes this destabilization.[50,57] Additionally, it has been reported that the destabilization arises from the displacement of water resulting from the strong binding of Ca^{2+} with phosphate moieties across the fusing bilayers.[54]

Our data provides new insights regarding the molecular mechanisms leading to a destabilization of the lipid bilayer. Our results agree with previous reports of PS lipids binding to Ca^{2+} in that with the inclusion of Mg^{2+}, the DPPS lipids maintain an ordered packing conformation to elevated temperatures.[37,61] Changes observed in the methylene deformation modes of the saturated acyl chains allow an assessment of the domain structure within the bilayer as a result of the binding of Mg^{2+} to the DPPS component. Our infrared spectroscopic measurements indicate specifically both a size and organizational change within the DPPS domains, as Mg^{2+} appears to organize the DPPS lipids into clusters of 10–15 lipids. The infrared spectra support Mg^{2+} binding to the phosphate of DPPS to form these micro-clusters. Within these DPPS domains there exists a packing configuration where the acyl chains exhibit a setting angle, related to the angle between the acyl chain planes and the orthorhombic subcell axis, approaching 20° as opposed to 40–50° in the absence Mg^{2+}. Despite no evidence of a direct interaction between DPPC and Mg^{2+}, The DPPC-d_{62} lipid domains also exhibit a change in acyl chain organization. That is, the frequency shift observed in the deuterated methylene deformation modes indicates that the DPPC lipids align with their acyl chain planes oriented in a parallel manner. In the absence of direct interaction between DPPC and Mg^{2+}, the observed

DPPC realignment likely results from a lateral force exerted within the bilayer arising from the DPPS/Mg^{2+} interaction. It has been noted that an important step in progressing from partial, or hemifusion, to complete fusion is an increase in the lateral tension within the lipid bilayer.[49] The increased free energy associated with bilayer tension is believed to destabilize the bilayer resulting in spontaneous pore formation. The infrared spectroscopic results presented here support such a mechanism; namely, when Mg^{2+} binds to DPPS to form a lipid cluster, increase in bilayer tension occurs. Pore formation arises when a critical concentration of DPPS domains are formed. The fusion mechanism suggested by the infrared measurements is supported by the light scattering and fluorescence measurements. In our lipid assemblies the degree of fusion observed in the light scattering studies is correlated with the percentage of DPPS relative to DPPC. At high DPPC concentrations, the threshold tension is not achieved, resulting only in vesicle aggregation, as observed, for example, in the 1:1 DPPS/DPPC assemblies.

Most reports of fusion in the literature involve Ca^{2+} as the fusion catalyst. The differences between Ca^{2+} and Mg^{2+} become important in model systems with respect to their binding to PS headgroups. It has been previously suggested that Ca^{2+} binds PS headgroups in a “trans” geometry, while Mg^{2+} creates a “cis” lipid complex.[55] The trans complex implicated binding through the carbonyl groups;[55] however, previous infrared spectroscopic studies showed the formation of bidentate Ca-PO_4 complex between Ca^{2+} and PS lipids.[37] The spectroscopic results presented here indicate that Mg^{2+} binds to PS in a similar fashion as Ca^{2+}. The reported Ca^{2+}/PS binding constant is reported to be double the Mg^{2+}/PS binding constant.[55] In the presence of Ca^{2+} PS lipids are reported to undergo a rapid phase separation, demixing in binary lipid model systems.[19,43,62] The systems reported in the present study do not indicate phase separation in the presence of Mg^{2+}. Specifically, the infrared spectroscopic melting curves in the presence of Mg^{2+} (Fig. 2) support a heterogeneous distribution of DPPC and DPPS lipid domains. This difference in Ca^{2+} and Mg^{2+} phase seperation behavior is likely related to the binding constant differences. The strong Ca^{2+}/PS binding results in virtually no free PS lipids when sufficient Ca is present; however, the lower Mg^{2+}/PS binding constant results in a fraction of unbound PS lipids in excess Mg^{2+}. It has been recognized that a principal difference between Ca^{2+} and Mg^{2+}, as reflected by the difference in binding constants, is the observed kinetics; such that Mg^{2+}/ PS binding occurs slower or requires higher cation concentrations.[50,55] The differences between Ca^{2+} and Mg^{2+} have been evaluated with respect to the surface tension needed to promote fusion, where the critical surface tensions needed were identical in both cases.[57] By avoiding phase separation in the model system presented in this study, the effects of divalent cation binding on the entire bilayer structure can be assessed. Since large-scale phase separation is not conducive to maintaining a stable membrane structure, our results offer a perspective into a mechanism that would be consistent with localized cation-lipid binding events, perhaps regulated *in vivo* by the cellular protein machinery. In vivo, Ca^{2+}, properly regulated, likely provides a more kinetically efficient response.

Simulations suggest that lipid bilayer fusion proceeds through the following pathway: contact (or stalk formation), formation of a hemifused system where the merging bilayers each contribute one leaflet though the contents remain separate, pore formation, followed by pore expansion that yields the fused state.[14,15,49,63–66] The PS – divalent cation interaction, as evidenced by the results presented here, appears to play a critical role throughout this process. Contact appears to be achieved through an electrostatic interaction, as evidenced by aggregation, with fusion only being observed in lipid assemblies containing the negatively charged PS headgroup. Interestingly, once bound to PS, the divalent cation appears to bind the phosphate groups preferentially. The binding event is reported to release water molecules, previously coordinated to both the divalent cation and the phosphate moiety, thus increasing the general hydrophobic character of the region.[54] An increasingly hydrophobic area would facilitate lipid rearrangements proceeding toward the formation of the hemifused state. Once in the hemifused state, the lateral tension induced by the PS domains (vida supra) result in the

formation of a pore. The alignment of the lipids, reflected by the change in setting angle throughout the bilayer assembly, facilitates the expansion of the pore into the final fused state.

To our knowledge, this realignment of the acyl chains within lipid assemblies in the presence of a divalent cation has not been previously demonstrated. In the present study saturated lipid acyl chains were used to give rise to clear correlation field splitting components for determining microdomain sizes; however, for assessing the details of acyl chain microdomain behavior in the future, investigations could extend to model systems involving unsaturated acyl chains, polyvalent headgroups, and other lipids found in intact biological membranes. Similarly, future work examining the role of fusion proteins in combination with diverse lipids may aid in clarifying the complex lipid rearrangement mechanisms that lead to *in vivo* membrane fusion.

5. Conclusion

The data presented here provide additional insights regarding the bilayer interactions between DPPS and DPPC lipids in response to a membrane fusion catalyst. Our results indicate that single shell vesicles comprised of binary assemblies of DPPS and DPPC fuse in the presence of a divalent Mg^{2+} cation. Inspection of the acyl chain infrared spectroscopic melting curves indicates the existence of DPPS and DPPC microdomains distributed throughout the bilayer. In the presence of Mg^{2+}, DPPS maintains a gel phase configuration above the phase transition. Analysis of the acyl chain methylene deformation modes demonstrate that interactions between DPPS head groups and a divalent cation, such as Mg^{2+}, result in microdomain formation and a rearrangement tendency of the acyl chain planes within the bilayer cluster. DPPC does not exhibit a response to the Mg^{2+} cation; however the DPPC acyl chains rearrange in a manner consistent with the DPPS matrix. Large quantities of DPPC in the bilayer assembly inhibit fusion. In summary, we suggest that the lipid reorganizations within predominantly DPPS lipid microdomains are critical in order to mechanistically drive the bilayer to a fused membrane state.

Supplementary Material

Refer to Web version on PubMed Central for supplementary material.

Acknowledgement

The authors thank Dr. Shuko Yoshikami for assistance preparing vesicles containing fluorescence indicators. This work was funded through the NIDDK intramural research program.

References

1. Jacobson K, Mouritsen OG, Anderson RGW. Lipid rafts: at a crossroad between cell biology and physics. Nat Cell Biol 2007;9:7. [PubMed: 17199125]
2. Brown DA. Lipid rafts, detergent-resistant membranes, and raft targeting signals. Physiology 2006;21:430. [PubMed: 17119156]
3. Lagerholm BC, Weinreb GE, Jacobson K, Thompson NL. Detecting Microdomains in Intact Cell Membranes. Annu. Rev. Phys. Chem 2005;56:309. [PubMed: 15796703]
4. Engelman DM. Membranes are more mosaic than fluid. Nature 2005;438:578. [PubMed: 16319876]
5. Vereb G, Szollosi J, Matko J, Nagy P, Farkas T, Vigh L, Matyus L, Waldmann TA, Damjanovich S. Dynamic, yet structured: The cell membrane three decades after the Singer-Nicolson model. Proc. Nat. Acad. Sci. USA 2003;100:8053. [PubMed: 12832616]
6. Brown DA, Rose JK. Sorting of Gpi-Anchored Proteins to Glycolipid-Enriched Membrane Subdomains During Transport to the Apical Cell-Surface. Cell 1992;68:533. [PubMed: 1531449]
7. Chan Y-HM, Boxer SG. Model membrane systems and their applications. Curr. Opin. Chem. Biol 2007;11:581. [PubMed: 17976391]

8. London E. How principles of domain formation in model membranes may explain ambiguities concerning lipid raft formation in cells. Biochim. Biophys. Acta 2005;1746:203. [PubMed: 16225940]
9. Edidin M. The state of lipid rafts: From model membranes to cells. Annu. Rev. Biophys. Biomol. Struct 2003;32:257. [PubMed: 12543707]
10. Edidin M. Lipids on the frontier: a century of cell-membrane bilayers. Nat. Rev. Mol. Cell Biol 2003;4:414. [PubMed: 12728275]
11. Feigenson GW, Buboltz JT. Ternary phase diagram of dipalmitoyl-PC/dilauroyl-PC/cholesterol: Nanoscopic domain formation driven by cholesterol. Biophys. J 2001;80:2775. [PubMed: 11371452]
12. Radhakrishnan A, Anderson TG, McConnell HM. Condensed complexes, rafts, and the chemical activity of cholesterol in membranes. Proc. Natl. Acad. Sci. USA 2000;97:12422. [PubMed: 11050164]
13. Hao M, Mukherjee S, Maxfield FR. Cholesterol depletion induces large scale domain segregation in living cell membranes. Proc. Natl. Acad. Sci. USA 2001;98:13072. [PubMed: 11698680]
14. Katsov K, Muller M, Schick M. Field Theoretic Study of Bilayer Membrane Fusion. I. Hemifusion Mechanism. Biophys. J 2004;87:3277. [PubMed: 15326031]
15. Kozlovsky Y, Kozlov MM. Stalk Model of Membrane Fusion: Solution of Energy Crisis. Biophys. J 2002;82:882. [PubMed: 11806930]
16. Weinreb G, Lentz BR. Analysis of Membrane Fusion as a Two-State Sequential Process: Evaluation of the Stalk Model. Biophys. J 2007;92:4012. [PubMed: 17369418]
17. Duzgunes N, Wilschut J, Fraley R, Papahadjopoulos D. Studies on the mechanism of membrane fusion. Role of head-group composition in calcium- and magnesium-induced fusion of mixed phospholipid vesicles. Biochim. Biophys. Acta 1981;642:182. [PubMed: 7225377]
18. Pantazatos DP, MacDonald RC. Directly Observed Membrane Fusion Between Oppositely Charged Phospholipid Bilayers. J. Membr. Biol 1999;170:27. [PubMed: 10398758]
19. Silvius JR, Gagne J. Calcium-induced fusion and lateral phase separations in phosphatidylcholine-phosphatidylserine vesicles. Correlation by calorimetric and fusion measurements. Biochem 1984;23:3241.
20. Sanchez-Migallon MP, Aranda FJ, Gomez-Fernandez JC. The dissimilar effect of diacylglycerols on Ca(2+)-induced phosphatidylserine vesicle fusion. Biophys. J 1995;68:558. [PubMed: 7696508]
21. Massari S, Folena E, Ambrosin V, Schiavo G, Colonna R. pH-dependent lipid packing, membrane permeability and fusion in phosphatidylcholine vesicles. Biochim Biophys. Acta 1991;1067:131. [PubMed: 1878366]
22. Ogawa Y, Kodaka M, Okuno H. Trigger lipids inducing pH-dependent liposome fusion. Chemistry and Physics of Lipids 2002;119:51. [PubMed: 12270673]
23. Higashino Y, Matsui A, Ohki K. Membrane fusion between liposomes composed of acidic phospholipids and neutral phospholipids induced by melittin: A differential scanning calorimetric study. J. Biochem., Tokyo 2001;130:393. [PubMed: 11530015]
24. Burgess SW, McIntosh TJ, Lentz BR. Modulation of Poly(Ethylene Glycol)-Induced Fusion by Membrane Hydration - Importance of Interbilayer Separation. Biochem 1992;31:2653. [PubMed: 1547208]
25. Johnsson M, Edwards K. Phase behavior and aggregate structure in mixtures of dioleoylphosphatidylethanolamine and poly(ethylene glycol)-lipids. Biophys. J 2001;80:313. [PubMed: 11159404]
26. Chanturiya A, Chernomordik LV, Zimmerberg J. Flickering fusion pores comparable with initial exocytotic pores occur in protein-free phospholipid bilayers. Proc. Natl. Acad. Sci. USA 1997;94:14423. [PubMed: 9405628]
27. Dibble AR, Hinderliter AK, Sando JJ, Biltonen RL. Lipid lateral heterogeneity in phosphatidylcholine/phosphatidylserine/diacylglycerol vesicles and its influence on protein kinase C activation. Biophys. J 1996;71:1877. [PubMed: 8889163]
28. Kraayenhof R, Sterk GJ, Wong Fong Sang HW, Krab K, Epand RM. Monovalent cations differentially affect membrane surface properties and membrane curvature, as revealed by fluorescent probes and dynamic light scattering. Biochim. Biophys. Acta 1996;1282:293. [PubMed: 8703985]

29. Roldan-Vargas S, Martin-Molina A, Quesada-Perez M, Barnadas-Rodriguez R, Estelrich J, Callejas-Fernandez J. Aggregation of liposomes induced by calcium: A structural and kinetic study. Phys. Rev. E 2007;75
30. van Dijck PWM, de Kruijff B, Verkleij AJ, van Deenen LLM, de Gier J. Comparative studies on the effects of pH and Ca2+ on bilayers of various negatively charged phospholipids and their mixtures with phosphatidylcholine. Biochim. Biophys. Acta 1978;512:84. [PubMed: 29665]
31. Luna EJ, McConnell HM. Lateral phase separations in binary mixtures of phospholipids having different charges and different crystalline structures. Biochim. Biophys. Acta 1977;470:303. [PubMed: 578776]
32. Yang L, Huang HW. Observation of a Membrane Fusion Intermediate Structure. Science 2002;297:1877. [PubMed: 12228719]
33. Yang L, Ding L, Huang HW. New Phases of Phospholipids and Implications to the Membrane Fusion Problem. Biochem 2003;42:6631. [PubMed: 12779317]
34. Snyder RG, Liang GL, Strauss HL, Mendelsohn R. IR spectroscopic study of the structure and phase behavior of long-chain diacylphosphatidylcholines in the gel state. Biophys. J 1996;71:3186. [PubMed: 8968589]
35. Hubner W, Mantsch HH, Paltauf F, Hauser H. Conformation of Phosphatidylserine in Bilayers as Studied by Fourier-Transform Infrared-Spectroscopy. Biochem 1994;33:320. [PubMed: 8286353]
36. López-García F, Micol V, Villalaín J, Gómez-Fernández JC. Infrared spectroscopic study of the interaction of diacylglycerol with phosphatidylserine in the presence of calcium. Biochim Biophys. Acta 1993;1169:264. [PubMed: 7548120]
37. Dluhy R, Cameron DG, Mantsch HH, Mendelsohn R. Fourier transform infrared spectroscopic studies of the effect of calcium ions on phosphatidylserine. Biochem 1983;22:6318.
38. Schultz ZD, Levin IW. Lipid Microdomain formation: Characterization by infrared spectroscopy and ultrasonic velocimetry. Biophys. J 2008;94:3104. [PubMed: 18192352]
39. Kirchhoff WH, Levin IW. Description of the Thermotropic Behavior of Membrane Bilayers in Terms of Raman Spectral Parameters - a 2-State Model. Journal of Research of the National Bureau of Standards 1987;92:113.
40. Kaszuba M, Connah MT, McNeil-Watson FK, Nobbmann U. Resolving concentrated particle size mixtures using dynamic light scattering. Particle & Particle Systems Characterization 2007;24:159.
41. Kodati VR, El-Jastimi R, Lafleur M. Contribution of the Intermolecular Coupling and Librotorsional Mobility in the Methylene Stretching Modes in the Infrared Spectra of Acyl Chains. J. Phys. Chem 1994;98:12191.
42. Caffrey, M. LIPIDAT: A Database of Thermodynamic Data and Associated Information on Lipid Mesomorphic and Polymorphic Transitions. Boca Raton: CRC Press, Inc.; 1993. Pages
43. Hinderliter AK, Huang J, Feigenson GW. Detection of phase separation in fluid phosphatidylserine/phosphatidylcholine mixtures. Biophys. J 1994;67:1906. [PubMed: 7858127]
44. Huang J, Swanson JE, Dibble AR, Hinderliter AK, Feigenson GW. Nonideal mixing of phosphatidylserine and phosphatidylcholine in the fluid lamellar phase. Biophys. J 1993;64:413. [PubMed: 8457667]
45. Rodriguez Y, Mezei M, Osman R. Association Free Energy of Dipalmitoylphosphatidylserines in a Mixed Dipalmitoylphosphatidylcholine Membrane. Biophys. J 2007;92:3071. [PubMed: 17277191]
46. Lewis, RNAH.; McElhaney, RN. Vibrational Spectroscopy of Lipids. In: Griffiths, JMCaPR., editor. Handbook of Vibrational Spectroscopy: Applications in Life, Pharmaceutical and Natural Sciences. Vol. Vol. 5. Chichester: John Wiley & Sons Ltd; 2002. p. 3447
47. Snyder RG, Goh MC, Srivatsavoy VJP, Strauss HL, Dorset DL. Measurement of the Growth-Kinetics of Microdomains in Binary N-Alkane Solid-Solutions by Infrared-Spectroscopy. J. Phys. Chem 1992;96:10008.
48. Snyder RG. Vibrational Spectra of Crystalline N-Paraffins .2. Intermolecular Effects. J. Mol. Spectrosc 1961;7:116.
49. Cohen FS, Melikyan GB. The Energetics of Membrane Fusion from Binding, through Hemifusion, Pore Formation, and Pore Enlargement. J. Membr. Biol 2004;199:1. [PubMed: 15366419]

50. Duzgunes N, Nir S, Wilschut J, Bentz J, Newton C, Portis A, Papahadjopoulos D. Calcium- and magnesium-induced fusion of mixed phosphatidylserine/phosphatidylcholine vesicles: Effect of ion binding. 1981;59:115.
51. Hark S-K, Ho JT. Raman study of calcium-induced fusion and molecular segregation of phosphatidylserine/dimyristoyl phosphatidylcholine-d54 membranes. Biochim. Biophys. Acta 1980;601:54. [PubMed: 7407165]
52. Sun ST, Hsang CC, Day EP, Ho JT. Fusion of phosphatidylserine and mixed phosphatidylserine-phosphatidylcholine vesicles Dependence on calcium concentration and temperature. Biochim. Biophys. Acta 1979;557:45. [PubMed: 549643]
53. Silvius JR. Calcium-induced lipid phase separations and interactions of phosphatidylcholine/anionic phospholipid vesicles. Fluorescence studies using carbazole-labeled and brominated phospholipids. Biochem 1990;29:2930. [PubMed: 2337575]
54. Jena, BP. Chapter 9 Understanding Membrane Fusion: Combining Experimental and Simulation Studies Methods in Cell Biology. In: Jena, BP., editor. Methods in Nano Cell Biology. Vol. Volume 90. Academic Press; 2008. p. 183
55. Portis A, Newton C, Pangborn W, Papahadjopoulos D. Studies on the Mechanism of Membrane-Fusion - Evidence for an Inter-Membrane Ca2+-Phospholipid Complex, Synergism with Mg2+, and Inhibition by Spectrin. Biochem 1979;18:780. [PubMed: 420815]
56. Papahadjopoulos D, Vail WJ, Jacobson K, Poste G. Cochleate Lipid Cylinders - Formation by Fusion of Unilamellar Lipid Vesicles. Biochim. Biophys. Acta 1975;394:483. [PubMed: 805602]
57. Ohki SA. Mechanism of Divalent Ion-Induced Phosphatidylserine Membrane-Fusion. Biochim. Biophys. Acta 1982;689:1. [PubMed: 7104344]
58. Jena, BP. Chapter 8 Assembly and Disassembly of SNAREs in Membrane Fusion Methods in Cell Biology. In: Jena, BP., editor. Methods in Nano Cell Biology. Vol. Volume 90. Academic Press; 2008. p. 157
59. Yoon T-Y, Lu X, Diao J, Lee S-M, Ha T, Shin Y-K. Complexin and Ca2+ stimulate SNARE-mediated membrane fusion. Nat Struct Mol Biol 2008;15:707. [PubMed: 18552825]
60. Wong JL, Koppel DE, Cowan AE, Wessel GM. Membrane Hemifusion Is a Stable Intermediate of Exocytosis. Dev. Cell 2007;12:653. [PubMed: 17420001]
61. Roux M, Bloom M. Calcium binding by phosphatidylserine headgroups. Deuterium NMR study. Biophys. J 1991;60:38. [PubMed: 1883944]
62. Ross M, Steinem C, Galla H-J, Janshoff A. Visualization of Chemical and Physical Properties of Calcium-Induced Domains in DPPC/DPPS Langmuir-Blodgett Layers. Langmuir 2001;17:2437.
63. Chernomordik LV, Zimmerberg J, Kozlov MM. Membranes of the world unite! J. Cell Biol 2006;175:201. [PubMed: 17043140]
64. Chernomordik LV, Kozlov MM. Membrane Hemifusion: Crossing a Chasm in Two Leaps. Cell 2005;123:375. [PubMed: 16269330]
65. Jahn R, Lang T, Südhof TC. Membrane Fusion. Cell 2003;112:519. [PubMed: 12600315]
66. Kozlovsky Y, Chernomordik LV, Kozlov MM. Lipid Intermediates in Membrane Fusion: Formation, Structure, and Decay of Hemifusion Diaphragm. Biophys. J 2002;83:2634. [PubMed: 12414697]

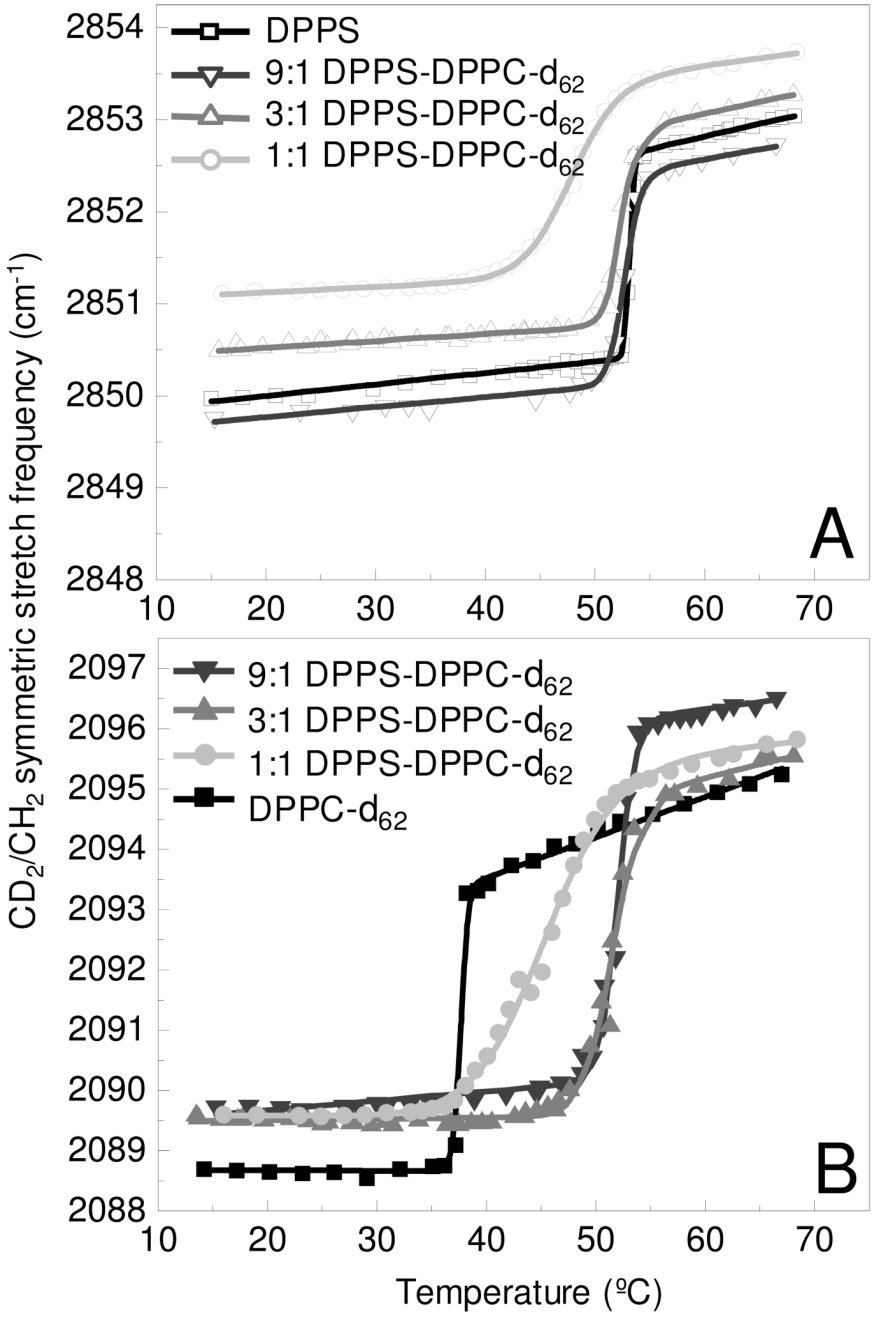

Figure 1.

Melting curves determine from the methylene symmetric stretching modes are shown for the DPPS MLVs (A) and DPPC-d_{62} MLVs (B) components in the binary bilayer assemblies. Melting curves are shown for the a pure lipid assembly (black) and mixed lipid assemblies comprised of 9:1 (dk. gray), 3:1 (gray), and 1:1 (lt. gray) DPPS – DPPC-d_{62}, respectively. Lines represent the fit to a two-state model. [39]

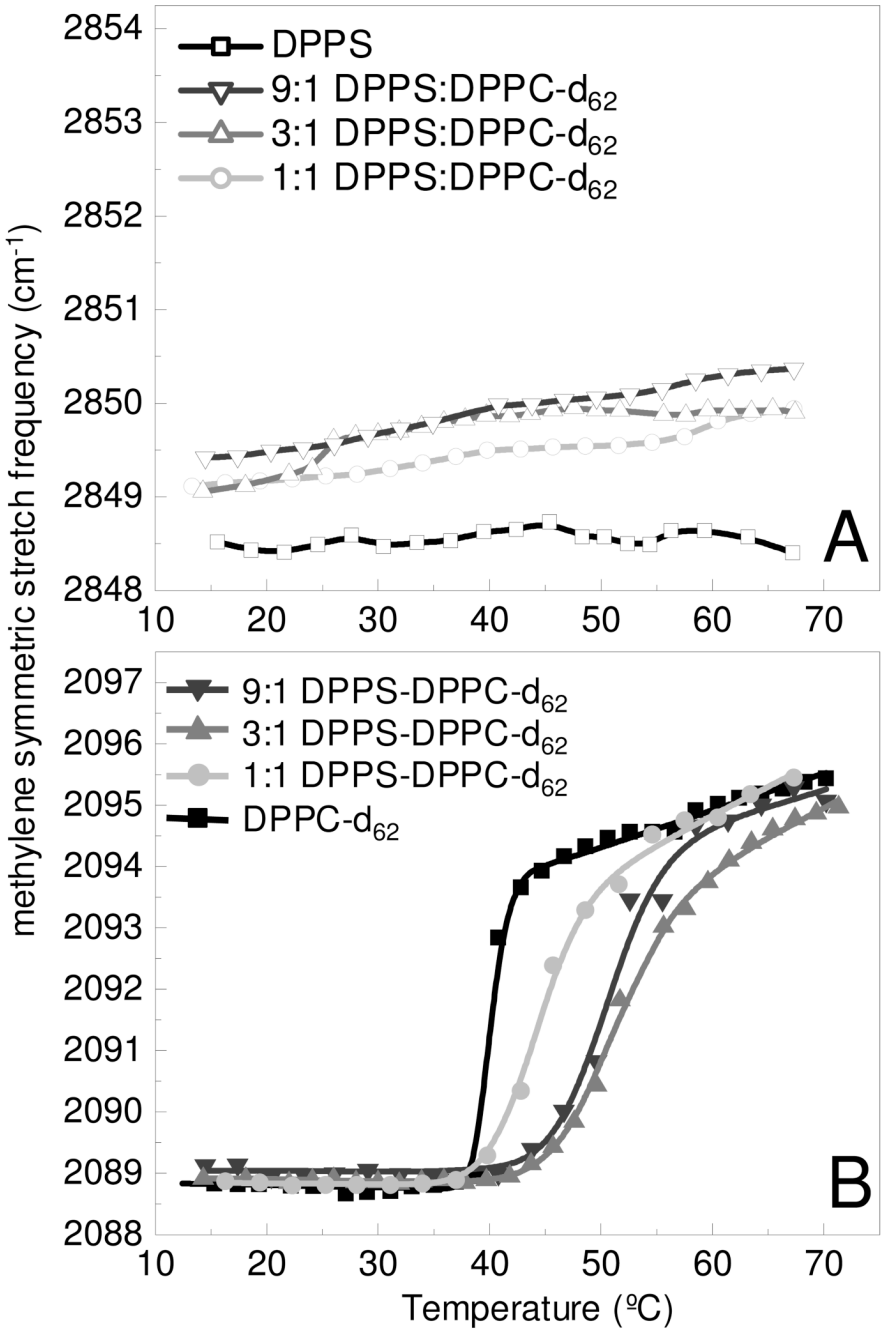

Figure 2.

Melting curves in the presence of Mg^{2+} are determined from the methylene symmetric stretching modes are shown for the DPPS MLVs (A) and DPPC-d_{62} MLVs (B) components in the binary bilayer assemblies. Melting curves are shown for the a pure lipid assembly (black) and mixed lipid assemblies comprised of 9:1 (dk. gray), 3:1 (gray), and 1:1 (lt. gray) DPPS – DPPC-d_{62}, respectively. The lines in panel B represent the fit to a two-state model.[39]

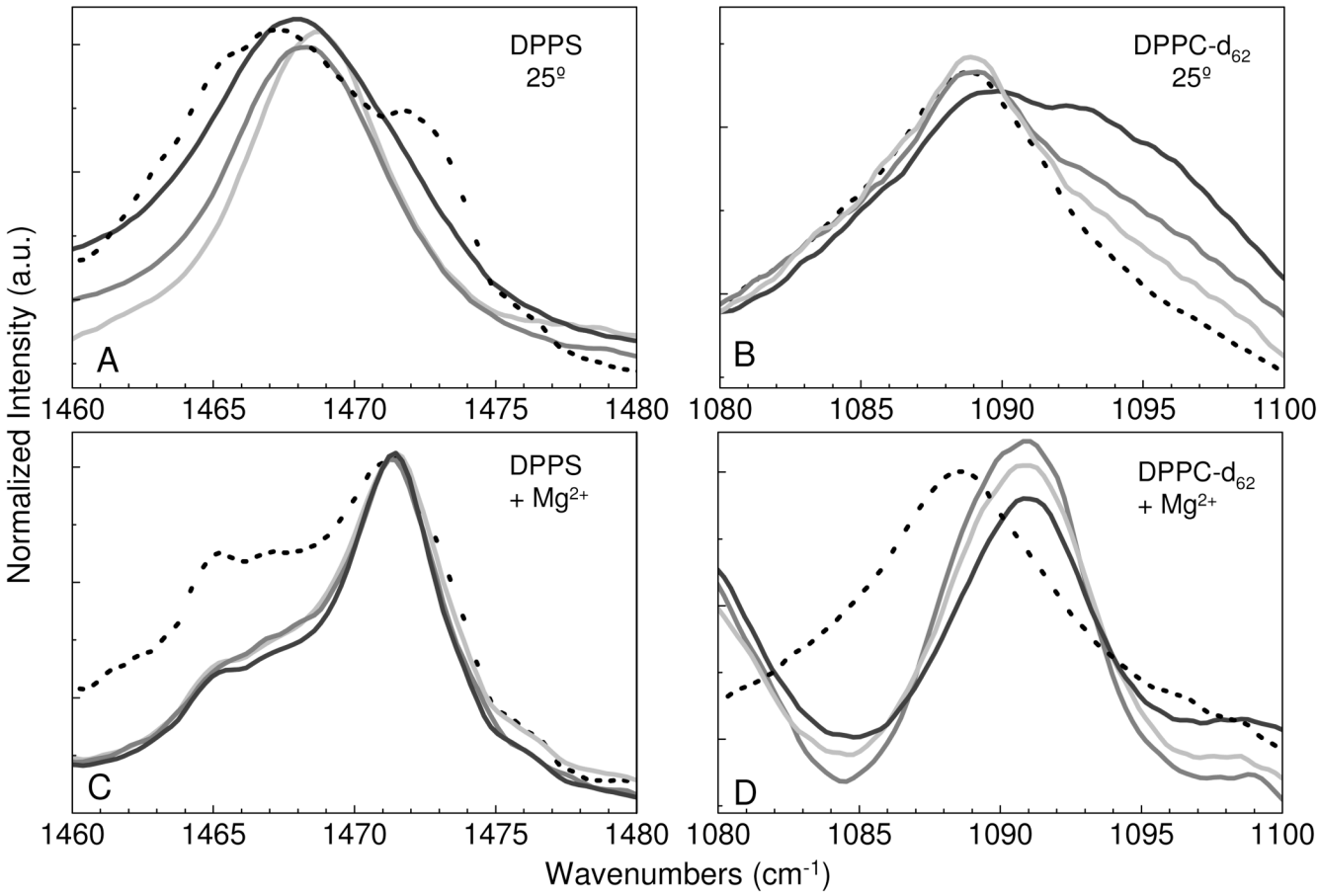

Figure 3.

For the binary systems the infrared spectra of the methylene deformation modes are shown at 25 °C for DPPS MLVs (A), DPPC-d_{62} MLVs (B), DPPS MLVs + Mg^{2+} (C), and DPPC-d_{62} MLVs +Mg^{2+} (D). Pure lipid MLV assemblies are represented by the black broken line, while the mixed lipid MLV assemblies are represented as follows: 9:1 (dk. gray), 3:1 (gray), and 1:1 (lt. gray) of DPPS – DPPC-d_{62}, respectively.

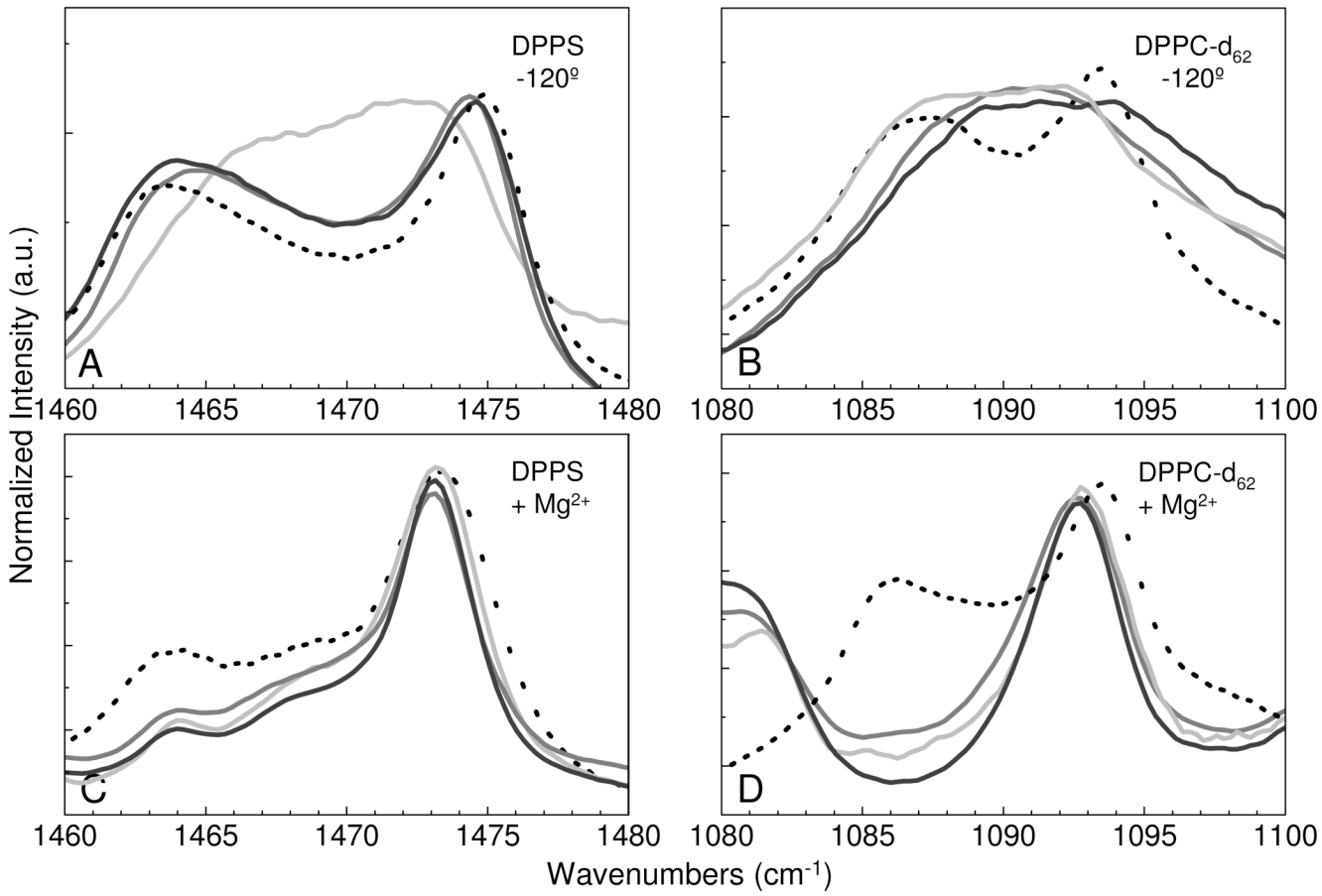

Figure 4.

For the binary systems the infrared spectra of the methylene deformation modes are shown at − 120 °C for DPPS MLVs (A), DPPC-d_{62} MLVs (B), DPPS MLVs + Mg^{2+} (C), and DPPC-d_{62} MLVs +Mg^{2+} (D). Pure lipid MLV assemblies are represented by the black broken line, while the mixed lipid MLV assemblies are represented as follows: 9:1 (dk. gray), 3:1 (gray), and 1:1 (lt. gray) of DPPS – DPPC-d_{62}, respectively.

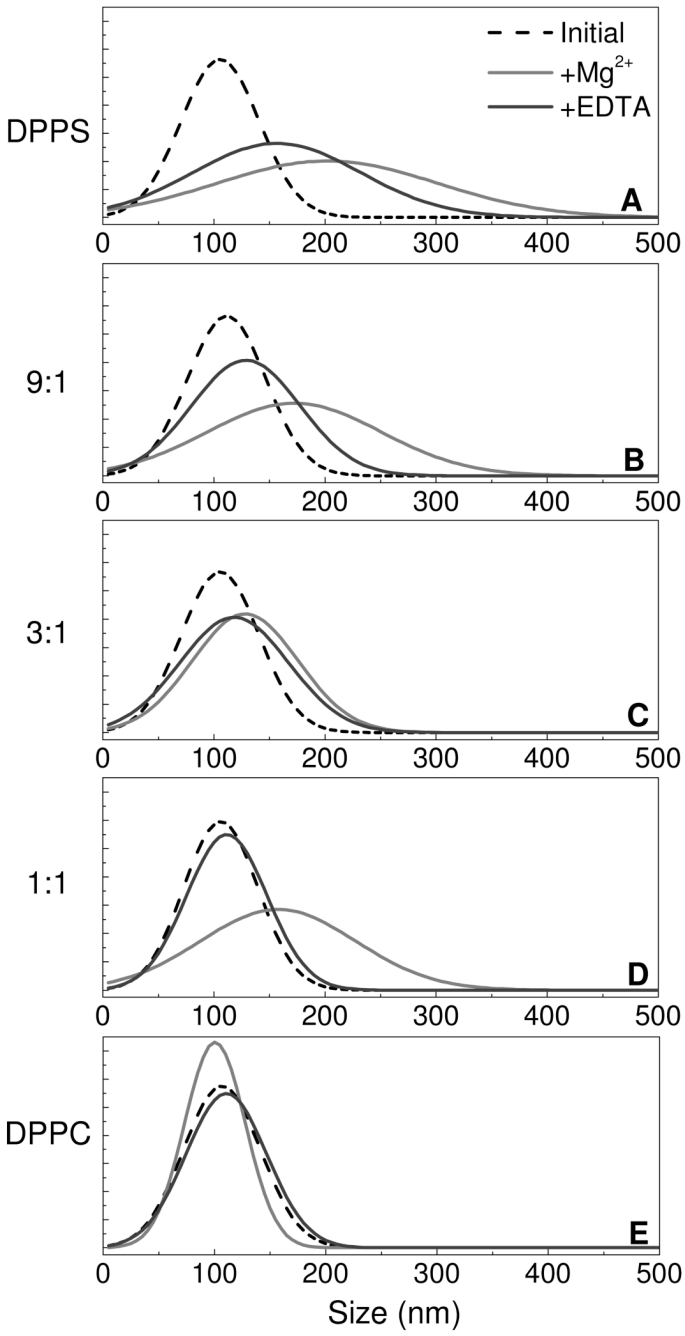

Figure 5.

The single shell size distributions for DPPS (A), the mixed lipid vesicle assemblies comprised of 9:1 (B), 3:1 (C), and 1:1 (D) DPPS – DPPC, respectively, and DPPC single shell vesicles (E) are plotted. The initial distribution is plotted in black (--), the distribution measured following the addition 1 mM Mg^{2+} is shown in gray (−), and the distribution resulting from the subsequent addition of excess EDTA is shown in dk. gray (−).

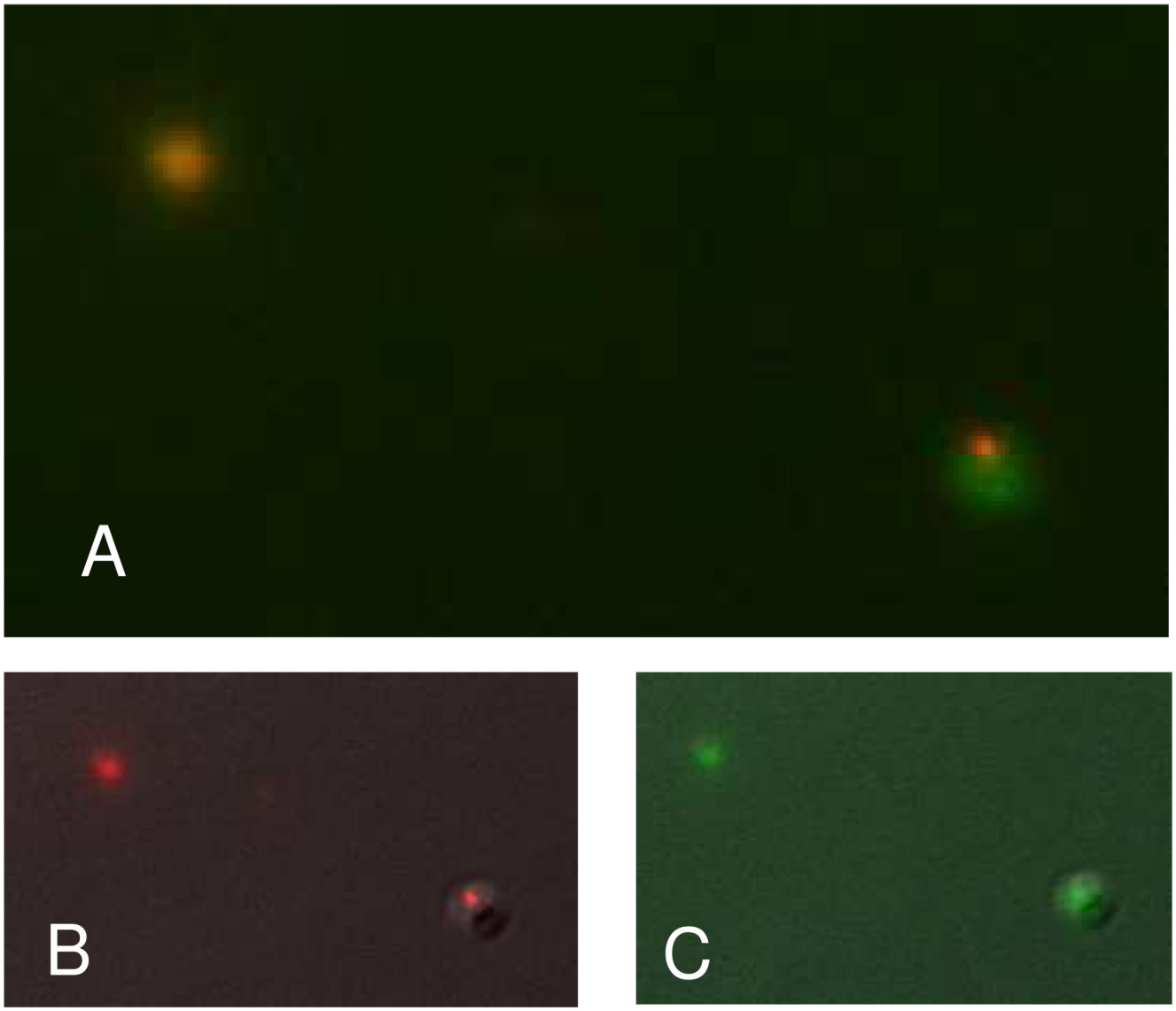

Figure 6.

The fluorescence image (A) obtained from a mixture of vesicles containing either 6-CF or SR101 combined in the presence of Mg^{2+} indicates both fusion and aggregation occurring as evidenced by the colocalization of the dyes but also the observation of aggregation products. The individual fluorescence signals are shown for SR101 (B) and 6-CF (C).

Table 1

Gel to liquid crystalline phase change temperatures and melting transition widths.

	DPPS		DPPC-d_{62}		DPPS + Mg^{2+}		DPPC-d_{62} + Mg^{2+}	
	T_m (°C)[a]	ΔT (°C)[b]	T_m (°C)[a]	ΔT (°C)[b]	T_m (°C)[a]	ΔT (°C)[b]	T_m (°C)[a]	ΔT (°C)[b]
DPPS	53.2 ± 0.1	0.8 ± 0.1	NA	NA	--	--	NA	NA
9 :1 DPPS-DPPC-d_{62}	52.7 ± 0.1	2.6 ± 0.1	52.0 ± 0.2	3.2 ± 0.2	--	--	50.3 ± 0.2	8.9 ± 0.4
3 :1 DPPS-DPPC-d_{62}	52.2 ± 0.1	2.6 ± 0.1	51.4 ± 0.2	5.0 ± 0.1	--	--	50.3 ± 0.1	10.7 ± 0.1
1 :1 DPPS-DPPC-d_{62}	47.8 ± 0.1	8.5 ± 0.1	45.2 ± 0.2	12.8 ± 0.1	--	--	43.7 ± 0.1	7.5 ± 0.2
DPPC-d_{62}	NA	NA	37.6 ± 0.1	0.7 ± 0.5	NA	NA	40.1 ± 0.1	1.8 ± 0.4

[a] T_m- Phase transition temperature

[b] ΔT – Melting transition width

Table 2

Methylene deformation mode correlation field splitting parameters at −120 °C, calculated domain sizes and setting angles.

	υ_a	υ_b	$\Delta\upsilon$	N[a]	I_a	I_b	I_a/I_b	θ[b]
DPPS	1474.7 ± 0.1	1463.5 ± 0.1	11.2 ± 0.1	--	0.134 ± 0.002	0.079 ± 0.09	1.70 ± 0.09	37°
9 :1	1474.7 ± 0.1	1463.5 ± 0.1	11.2 ± 0.1	>100	0.16 ± 0.04	0.12 ± 0.03	1.3 ± 0.5	41°
3 :1	1474.6 ± 0.1	1464.7 ± 0.1	9.9 ± 0.4	30	0.34 ± 0.05	0.4 ± 0.04	0.9 ± 0.2	50°
1 :1	1473.5 ± 0.1	1465.9 ± 0.1	7.6 ± 0.4	8	0.11 ± 0.1	0.13 ± 0.03	0.8 ± 0.4	50°
DPPC-d_{62}	1093.5 ± 0.1	1086.0 ± 0.1	7.5 ± 0.1	--	0.42 ± 0.01	0.35 ± 0.01	1.20 ± 0.04	42°
9 :1	1091.1 ± 0.1	--	--	*c*	--	--	--	--
3 :1	1089.3 ± 0.1	--	--	*c*	--	--	--	--
1 :1	1092.3 ± 0.1	1087.3 ± 0.1	5.1 ± 0.3	7	0.17 ± 0.03	0.28 ± 0.08	0.6 ± 0.2	52°
+Mg^{2+}								
DPPS	1473.3 ± 0.1	1463.4 ± 0.1	9.9 ± 0.1	30	0.15 ± 0.01	0.04 ± 0.01	3.8 ± 0.3	27°
9 :1	1473.2 ± 0.1	1463.8 ± 0.1	9.4 ± 0.1	20	0.53 ± 0.01	0.06 ± 0.01	8.9 ± 0.3	19°
3 :1	1473.1 ± 0.1	1463.7 ± 0.1	9.4 ± 0.1	20	0.49 ± 0.09	0.07 ± 0.01	7 ± 1	20°
1 :1	1473.3 ± 0.1	1463.8 ± 0.1	9.5 ± 0.1	22	0.47 ± 0.01	0.06 ± 0.01	7.5 ± 0.6	20°
DPPC-d_{62}	1093.6 ± 0.2	1085.8 ± 0.1	7.8 ± 0.2	--	0.20 ± 0.03	0.14 ± 0.02	1.4 ± 0.3	40°
9 :1	1092.6 ± 0.1	--	--	*d*	0.37 ± 0.01	--	--	--
3 :1	1092.5 ± 0.2	--	--	*d*	0.5 ± 0.1	--	--	--
1 :1	1092.8 ± 0.1	--	--	*d*	0.39 ± 0.02	--	--	--

[a] Calculated domain size, where N represents the number of interacting acyl chains.

[b] Calculated setting angle, where θ is related to the angle between the lipid acyl chain plane and the orthorhombic subcell axis.

[c] The broad peak observed is not amenable to analysis of correlation field splitting components used to determine microdomain sizes.

[d] Infrared spectroscopy cannot determine cluster sizes for lipid triclinic subcells.